The adsorbate state specific photochemistry of dioxygen on Pd(111)

Cite as: J. Chem. Phys. **93**, 5327 (1990); https://doi.org/10.1063/1.459652
Submitted: 05 March 1990 . Accepted: 19 June 1990 . Published Online: 04 June 1998

M. Wolf, E. Hasselbrink, J. M. White, and G. Ertl

The adsorbate state specific photochemistry of dioxygen on Pd(111)

M. Wolf, E. Hasselbrink, J. M. White,[a] and G. Ertl

Fritz-Haber-Institut der Max-Planck-Gesellschaft, Faradayweg 4-6, D-1000 Berlin 33, West Germany
(Received 5 March 1990; accepted 19 June 1990)

The ultraviolet-photochemistry of molecularly adsorbed oxygen on Pd(111) has been studied using pulsed laser light with 6.4 eV photon energy. Three processes occur upon irradiation: desorption of molecular oxygen, conversion between adsorption states, and dissociation to form adsorbed atomic oxygen. By using time-of-flight spectroscopy to detect the desorbing molecular oxygen and post-irradiation thermal desorption spectroscopy (TDS) to characterize the adsorbate state, a detailed picture of the photochemical processes is obtained. The data indicate that the O_2 molecules desorbing with low translational energies from the saturated surface as well as the conversion of adsorbed molecules between binding states are induced by the photoinduced build-up of atomic oxygen on the surface. Analysis of a proposed reaction model reproduces the observed data and yields detailed rates. Polarization analysis indicates that the photochemical processes are initiated by electronic excitations of the substrate.

I. INTRODUCTION

Only recently has it been established that electronic excitations in the valence band regime ($h\nu < 10$ eV) can lead to photochemical processes on metallic substrates which can compete effectively with the rapid quenching due to the nonradiative energy transfer to the metal.[1,2] The photochemistry of the methylhalides,[3,4] of nitrous (di)oxide[5,6,7,8] and dioxygen[9,10] have evolved as testing grounds for our understanding of these processes.

Having examined O_2 on Pd(111) we report here on the photodesorption and interconversion between adsorbate states initiated by irradition with 6.4 eV light. The results are complementary to those of a recent investigation by Hanley *et al.*[9] who studied the wavelength dependence of the photochemistry of dioxygen using cw light. By using pulsed lasers and combining thermal desorption spectroscopy (TDS) for probing the adsorbate state with time-of-flight (TOF) analysis of desorbing O_2 molecules, it becomes possible to derive a more complete picture of the photochemistry of this system. We put particular emphasis on the adsorbate state specific aspects of photoinduced desorption and conversion between adsorption states. Time-of-flight analysis of desorbing molecules allows to discriminate between direct, i.e., photochemical, desorption and desorption induced by rearrangement on the surface. Further, we report the desorption yield as function of polarization and angle of incidence, which gives insights into the excitation mechanism.

The adsorption of oxygen on palladium(111) has been studied using various experimental techniques. Adsorption of O_2 on Pd(111) at 100 K proceeds through population of three molecular adsorption states. These states and the desorption/dissociation processes connected with them have been characterized using TDS,[11] high resolution electron energy loss spectroscopy (HREELS)[12] and isotope exchange experiments.[11,13] TDS shows three molecular desorption processes, α_1–α_3, which can be associated with three molecularly chemisorbed species: superoxo ($\nu_{O\text{-}O} = 1035$ cm^{-1}), peroxo-I ($\nu_{O\text{-}O} = 850$ cm^{-1}) and peroxo-II ($\nu_{O\text{-}O} = 650$ cm^{-1}) with the O–O frequencies in brackets as observed by HREELS at similar temperatures (Table I). The assignments have been made based on similarities to organometallic compounds. All three species are believed to bind side-on to the Pd(111) surface.[12] The peroxo-I species is bound on top of a single Pd-atom, whereas the peroxo-II species is bridge bound. Although molecular oxygen adsorption is believed to be precursor mediated, physisorbed oxygen desorbs below 40 K. Thus no O_2 multilayers are formed at 90 K and the photolysis experiments reported here involve only the chemisorbed molecular oxygen species.

All studies indicate that thermal dissociation of molecular oxygen is negligible below 180 K. Upon heating above this temperature, desorption and dissociation occur simultaneously, provided the total coverage of O_2 exceeds 20% of the saturation value at 100 K. The dissociated fraction forms adsorbed atomic oxygen.

Matsushima[11] has also studied the coadsorption of atomic oxygen with molecular species. The saturation coverage of atomic oxygen is 0.25 ML. Preadsorbed atomic oxygen prevents completely the adsorption of α_1–$O_2(a)$ and

TABLE I. Summary of chemisorbed oxygen data.

	superoxo (α_3)	peroxo-I (α_2)	peroxo-II (α_1)
Desorption temperature[a] [K]	120	155	200
Saturation coverage [ML]	0.06	0.17	0.39
$\nu_{O\text{-}O}$ [cm^{-1}]	1 035	850	650
Charge transfer	1	1.3	1.7

[a] The differences in the desorption temperatures reported by the individual authors can be attributed to the various heating rates used (< 1–9 K/s).

[a] Permanent address: Department of Chemistry, University of Texas, Austin, Texas 78712.

 0021-9606/90/195327-10$03.00

partly of α_2–$O_2(a)$, whereas α_3–$O_2(a)$ remains almost unaffected.

Hanley *et al.*[9] have observed three processes upon irradiation with light of shorter wavelength than ~350 nm ($h\nu > 3.5 \pm 0.4$ eV): desorption of molecular oxygen, conversion between different molecular binding states and dissociation into atomic oxygen. With the highest photon energy applied, 5.2 eV, cross sections for photodesorption and dissociation of $1.3 \cdot 10^{-19}$ and $3.5 \cdot 10^{-20}$ cm^2, respectively, are reported. Similar processes have been observed on Pt(111)[10] and Ag(110).[14] In both studies the photolytical formation of atomic oxygen could directly be monitored by HREELS.

II. EXPERIMENT

The experiments were performed in an UHV-chamber which has been largely described elsewhere.[7] The apparatus was equipped with a LEED/AES unit, an Ar^+ sputter ion gun and a quadrupole mass spectrometer (QMS), which could be rotated around the sample. The Pd(111) crystal was cleaned with a standard procedure of Ar^+ bombardment and oxygen treatment at 800 K surface temperature. Adsorption of oxygen at room temperature and subsequent heating up to 1000 K was repeated until no desorption of CO could be monitored with the QMS and no impurities were detectable by AES.

The Pd(111) crystal was dosed at 90 K surface temperature with O_2 (Messer Griesheim, 99.998%) using a molecular beam. Line-of-sight thermal desorption spectra (TDS) were recorded at a heating rate of 3 K/s. The sample was irradiated with pulsed UV-light from an ArF-excimer laser (Lambda Physik, EMG 150 MSC) which outputs 6.4 eV (193 nm) radiation with 13 ns pulse duration. The laser fluence per pulse was typically kept below 2.5 mJ/cm^2 in order to prevent desorption due to thermal heating induced by absorbed light. Using the equations given by Burgess *et al.*[15] a maximum transient temperature rise of 10 K is predicted (13 ns pulse duration at $h\nu = 6.4$ eV). We will refer to the surface temperature between the laser pulses as surface idle temperature. If not otherwise noted, the sample was irradiated with nonpolarized light at normal incidence, but, if desired, a Rochon prism was used to obtain polarized light.

The yield of desorbing oxygen molecules initiated by a laser pulse was monitored with the QMS set at a selected desorption angle, typically 23.5° with respect to the surface normal. With this arrangement it was also possible to record time-of-flight (TOF) spectra. A crystal-to-ionizer distance of 54 mm was used. The data were correced for the ion flight time through the QMS (13 μs). The resulting spectra were fitted using a modified Maxwell-Boltzmann distribution

$$n(t) = at^{-4} \exp\left[-b\left(\frac{d}{t} - v_0\right)^2\right], \qquad (1)$$

where a is a normalization constant, b a measure of the translational energy, v_0 a flow velocity, d the distance between the crystal and the detection point. The velocity is connected to the flight distance and flight time by $v = d/t$. The flux-weighted mean translational energy, $\langle E_{\text{trans}} \rangle / 2k$, was then calculated by integration of the fit curve.[16]

III. RESULTS

A. Thermal desorption spectroscopy

Two series of thermal desorption spectra have been recorded. In the first case O_2 was adsorbed on the surface at 90 K up to saturation of all three states of molecular oxygen. Figure 1 shows a series of TD spectra after irradiation with various numbers of laser shots. Upon irradiation part of the α_1–$O_2(a)$ is converted to α_2– and α_3–$O_2(a)$, which becomes obvious from the increase of the α_3-peak. From the decrease of the total TDS area it must be concluded that $O_2(a)$ either dissociated to form atomic oxygen which appears in TDS only at higher temperatures, or desorbed into the gas phase. After a dose of $1.0 \cdot 10^{18}$ photons/cm^2 the population in α_1 is completely depleted. With further irradiation depletion continues with a higher rate for the α_2 species than for α_3–$O_2(a)$.

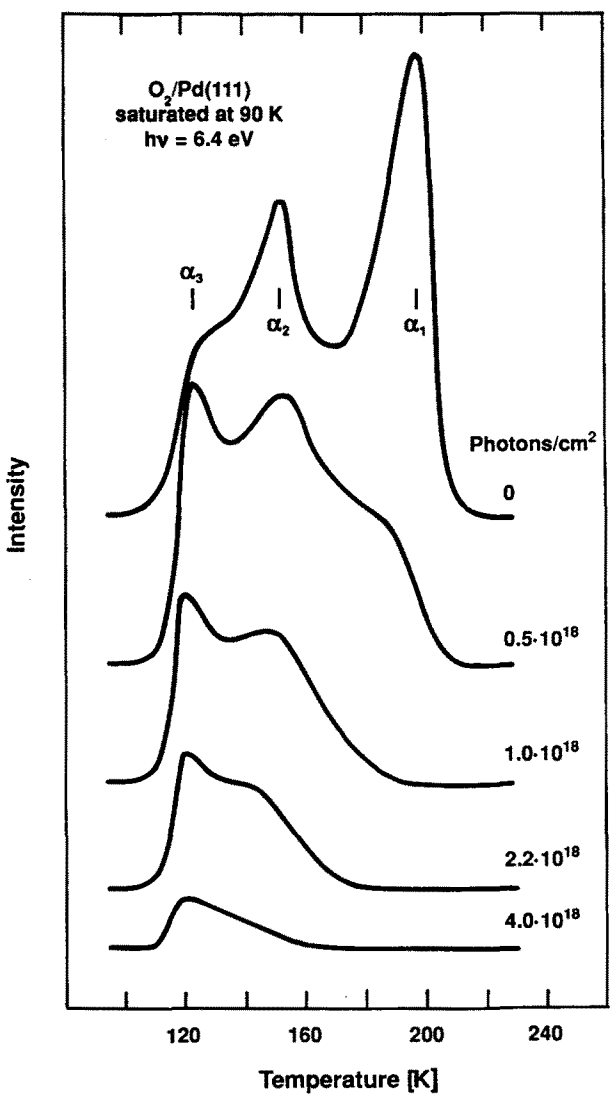

FIG. 1. Thermal desorption spectra of molecular oxygen adsorbed on Pd(111). The surface has been saturated with $O_2(a)$ at 90 K. The spectra were taken after various exposures to UV-laser light (6.4 eV) at 90 K surface idle temperature.

This interconversion of binding states from higher binding energy into lower binding energy becomes even more evident if initially only the α_1–$O_2(a)$ is prepared (achieved by dosing the crystal at 153 K). For the TD spectra shown in Fig. 2 the sample temperature has been reduced to 90 K after dosing at 153 K. The top trace shows that this procedure yields only population in α_1 and that there is no thermal conversion into the other states. Upon irradiation, first α_2– and then α_3–$O_2(a)$ are populated. Conversion appears to proceed stepwise: $\alpha_1 \rightarrow \alpha_2 \rightarrow \alpha_3$ as can be seen from the TDS traces after irradiation with $0.6 \cdot 10^{18}$ and $1.5 \cdot 10^{18}$ photons/cm^2 (Fig. 2). Parallel desorption also occurs, as becomes evident from quantitative analysis of the TDS data.

Figure 3 gives a systematic evaluation of the TDS areas from a larger number of spectra than shown in Fig. 1. The depletion of the total $O_2(a)$ TDS area starts with the first photons. A fit to the variation of adsorbed molecules, N, with the number of photons impinged on the surface, n_{ph}, with a simple exponential, $N = N_0 \exp(-\sigma n_{ph})$, yields a total cross section σ of $1.1 \cdot 10^{-18}$ cm^2 for the photoinduced loss of adsorbed O_2. The corresponding TDS areas of the α_2- and α_3-state first increase, at the expense of the α_1-population, and reach maxima after irradiation with 0.25 and $0.5 \cdot 10^{18}$ photons/cm^2, respectively.

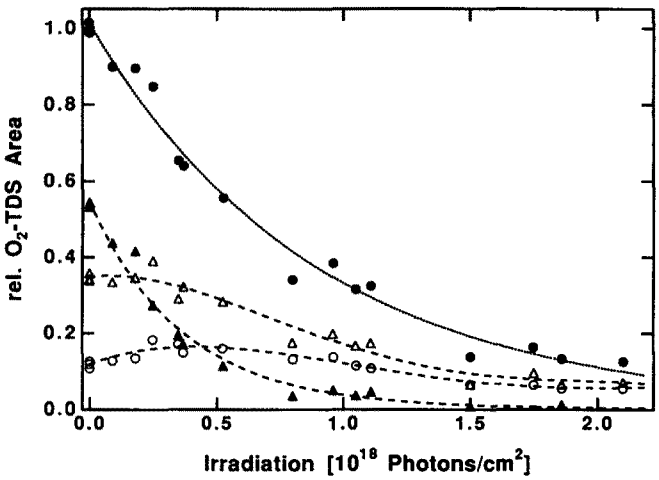

FIG. 3. Evaluation of the O_2 TDS areas (Fig. 1) vs photon exposure. The depletion of the total $O_2(a)$ TDS area (●) can be fitted with a single exponential decay leading to a total cross section of $1.1 \cdot 10^{-18}$ cm^2. Looking in more detail at the three molecular states it is seen that the populations in α_2(Δ) and α_3(○) go through an intermediate maximum at the expense of the population in α_1–$O_2(a)$ (▲). The lines are drawn to guide the eye.

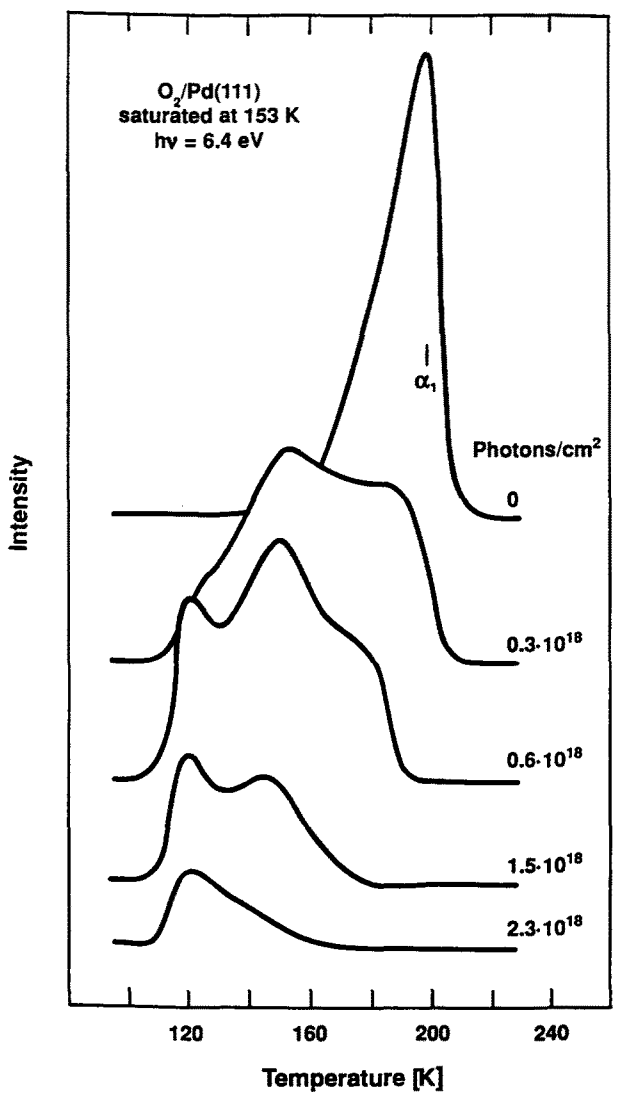

FIG. 2. Thermal desorption spectra of molecular oxygen adsorbed on Pd(111). The surface has been saturated with $O_2(a)$ at 153 K where only α_1–$O_2(a)$ is populated. The spectra were taken after various exposures to UV-laser light (6.4 eV) at 90 K surface idle temperature.

When only the α_1-species was initially populated, quite a different picture evolves (Fig. 4). With the first photons practically no reduction of the total TDS area is observed. Conversion from the α_1-species to α_2– and later α_3–$O_2(a)$ dominates. Only when these states are significantly populated does depletion of the total TDS area become evident. The α_2–$O_2(a)$ population peaks after irradiation with $0.5 \cdot 10^{18}$ photons/cm^2; α_3–$O_2(a)$ reaches its maximum slightly later.

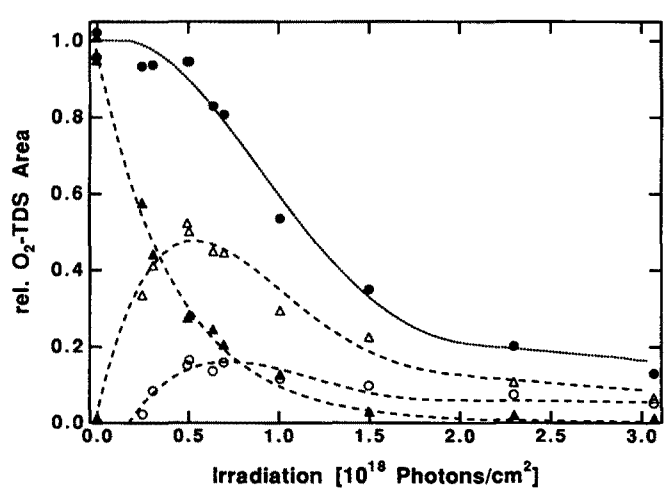

FIG. 4. Evaluation of the O_2 TDS areas (Fig. 2) vs photon exposure. Initially no depletion of the total $O_2(a)$ TDS area (●) is observed. α_1–$O_2(a)$ (▲) is converted into α_2(Δ) and later α_3–$O_2(a)$ (○). Depletion of the total coverage starts when α_2 and α_3 become significantly populated. The lines are drawn to guide the eye.

Atomic oxygen has been detected by coadsorbing molecular CO after annealing the surface to 220 K. TDS then shows CO_2 desorption around 400 K. The amount of released CO_2 is a measure of the atomic oxygen coverage, which can be calibrated by dosing oxygen at 300 K resulting in 0.25 ML O(a). The atomic oxygen observed can originate from two sources, thermal dissociation during heating the surface and photolysis by the laser radiation. For no irradiation, an atomic oxygen coverage of 0.21 ML is found. After irradiation with $2 \cdot 10^{18}$ photons/cm^2 there is a slight increase to 0.26 ML. Titration of atomic oxygen without prior annealing was not feasible, because dosing of CO lead to complete displacement of molecular oxygen and, simultaneously, dissociation to form atomic oxygen.

B. Time-of-flight spectroscopy

Time-of-flight spectroscopy provides deeper insights into the mechanism of the desorption process, because it reveals the details of the energetics of the fragmentation process. Starting with the surface saturated at 90 K, a series of consecutive TOF-spectra were recorded at 90 K idle temperature (Fig. 5). For each spectrum the signals resulting from 64 laser shots have been summed. This number of shots accounts for $0.17 \cdot 10^{18}$ photons/cm^2. The series of TOF-spectra shows hence the evolution of the velocity distribution with progressing irradiation. Velocity distributions are bimodal [Fig. 6(a)]. A fit to these spectra using a superposition of two modified Maxwell–Boltzmann distributions [Eq. (1)] yields for the average translational energy, $\langle E_{\text{trans}} \rangle / 2k$, 800 ± 50 and 120 ± 20 K for the fast and slow component, respectively. The obtained value for $\langle E_{\text{trans}} \rangle / 2k$ in the slow channel is close to the surface temperature during the laser pulse which will peak at 100 K, so that these molecules might be interpreted as being accommodated to the surface. $\langle E_{\text{trans}} \rangle / 2k$ for the fast channel is far in excess of the surface temperature and indicates therefore a nonthermal photodesorption channel. It has been checked that the position of the TOF-maxima scales properly with the crystal-to-ionizer distance, and that no spurious signals from temporal pressure rises are recorded.

The temporal position of the two contributions, and therefore the translational energy, does not significantly change as function of irradiation time. But obviously the intensity ratio of the two channels changes drastically. The flux weighted portion of the slow channel decreases within the first 10^{18} photons/cm^2 from 30% to less than 10%. At this point it becomes practically undecidable whether a slow channel still contributes and the data could as well be interpreted by assuming only a single channel. The time evolution of the TOF-signal can be better followed when the desorption signal per shot is directly recorded. Using a boxcar averager the signal for flight times between 40 and 105 μs has been integrated and averaged over 10 shots [Fig. 7(a)]. After a short period of constant signal it decreases exponentially. A fit to the exponential decay with $I = I_0 \cdot \exp(-\sigma n_{\text{ph}})$ yields a cross section of $1.05 \cdot 10^{-18}$ cm^2 which is practically the same value as obtained from the evaluation of the TDS areas. Also shown is the signal for the slow channel as obtained by combining the so-recorded data for the fast channel with the relative yields obtained from the fits to the TOF-spectra (Fig. 5).

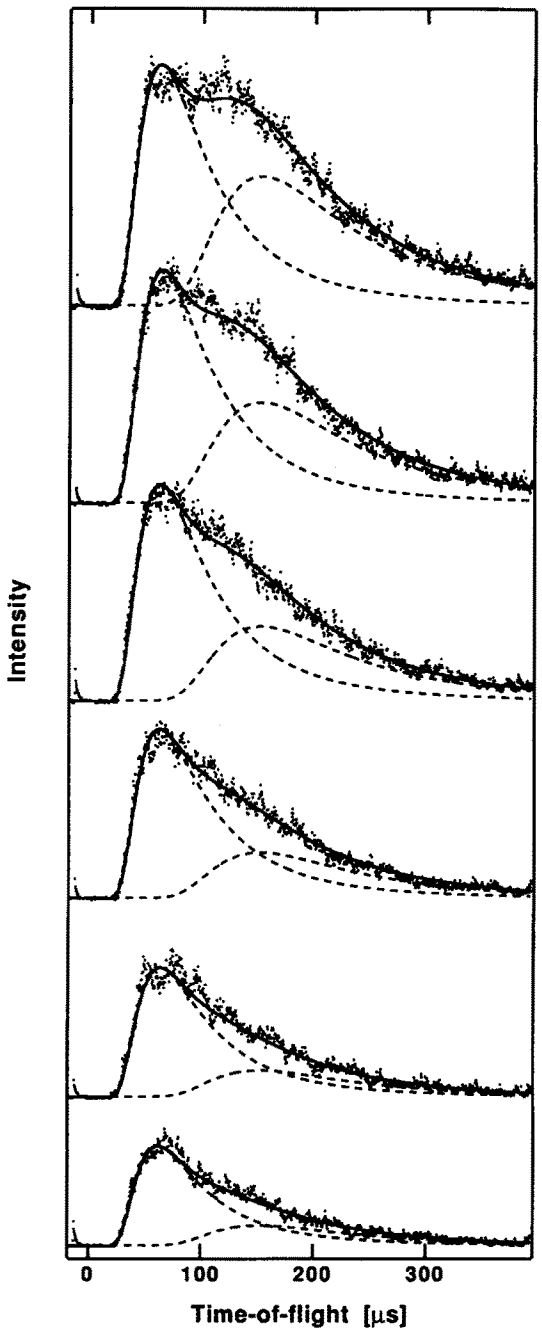

FIG. 5. Series (top to bottom) of consecutive time-of-flight (TOF) spectra for O_2 from a saturated surface at 90 K idle temperature. Each spectrum was averaged over 64 laser pulses ($0.17 \cdot 10^{18}$ photons/cm^2). The series shows the evolution of the time-of-flight spectrum with progressing irradiation. After the last spectrum (321st to 384th laser pulse) the total irradiation had been $1 \cdot 10^{18}$ photons/cm^2. The TOF distributions are clearly bimodal. The relative contribution from the slow channel decreases rapidly during irradiation from 30% (top) to finally less than 10% (bottom).

Starting with the α_1 state saturated at 153 K and irradiating at 90 K surface idle temperature the same procedure yields trace b of Fig. 7. The signal increases first and passes through a maximum after an exposure to $0.5 \cdot 10^{18}$ photons/cm^2. The observed maximum coincides with the maximum

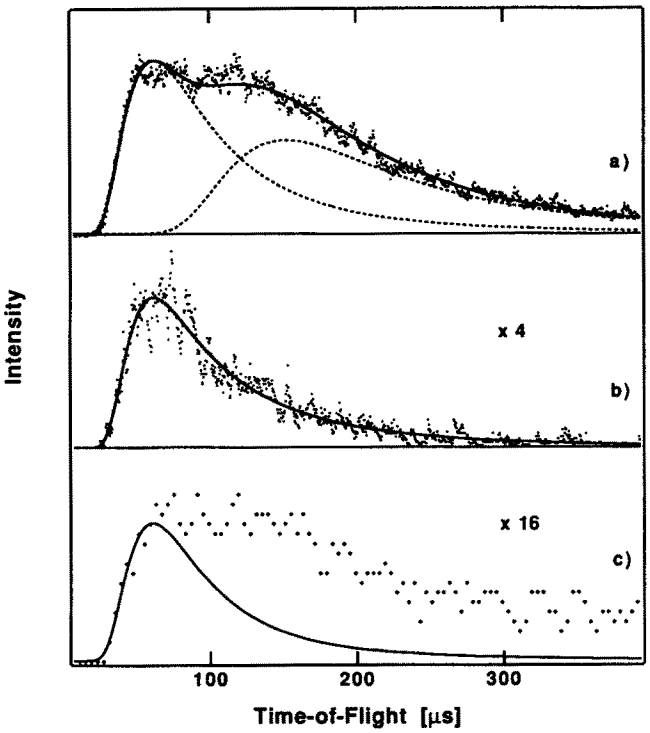

FIG. 6. (a) TOF-spectra for a saturated surface at 90 K, (b) a α_1-prepared surface irradiated at 90 K, and (c) at 153 K surface idle temperature. The solid lines represent fits by modified Maxwell–Boltzmann distributions. The mean translational energies $\langle E_{trans} \rangle / 2k$ of the desorbing O_2 molecules are 800 K and 120 K for the fast and slow channel, respectively. When only α_1 is prepared no contribution from the slow channel is seen at 90 K surface idle temperature. At (c) 153 K a fast signal is observed, but a broad thermal desorption is dominant. In this case the solid curve indicates a fast channel as inferred from the spectra above.

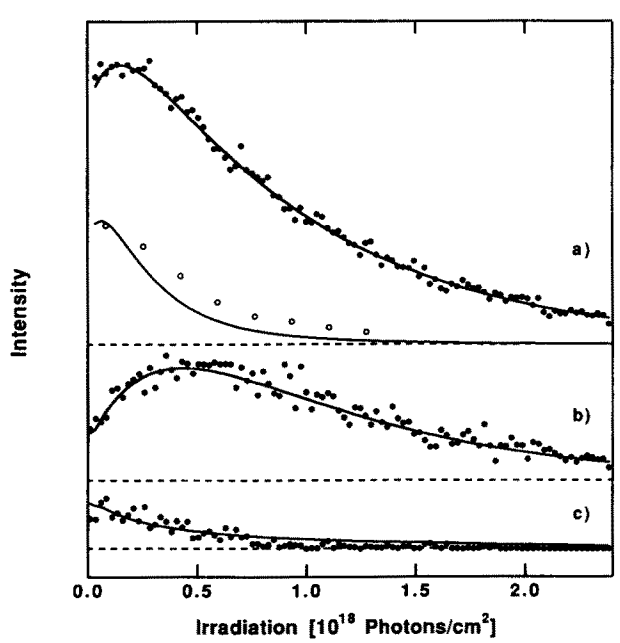

FIG. 7. Desorption signals vs irradiation. Top: surface saturated and irradiated at 90 K (●: fast channel; ○: slow channel). Middle: Only α_1–$O_2(a)$ saturated at 153 K and irradiated at 90 K. Bottom: Only α_1–$O_2(a)$ saturated and irradiated at 153 K. The solid lines give the results from the model discussed in Sec. IV.

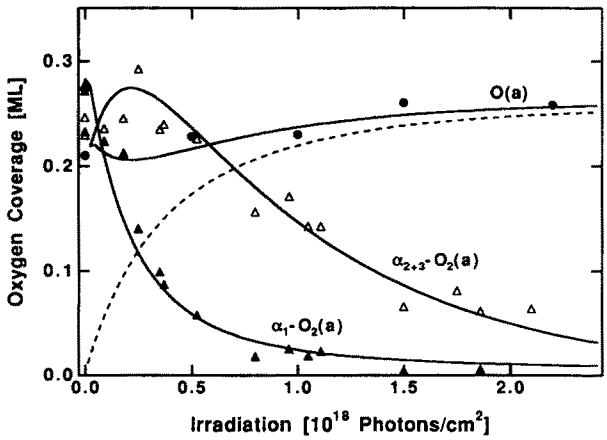

FIG. 8. Comparison of the TDS results for the saturated surface with a rate equation model: α_1–$O_2(a)$ (▲), α_{2+3}–$O_2(a)$ (△). Shown is also the total amount of atomic oxygen (●) detected after annealing to 220 K. The solid curves give the results of the rate model. The dashed curve shows the calculated amount of photoinduced atomic oxygen.

population of α_2– and α_3–$O_2(a)$ as monitored by TDS (Fig. 4). The observed TOF-spectra exhibit only the fast channel [Fig. 6(b)]. A similar time series as described above has been recorded for the surface prepared solely with the α_1-state. In this case all spectra can be consistently modelled assuming a single channel with $\langle E_{trans} \rangle / 2k = 800 \pm 50$ K. Trials to include a slow channel in the fit procedure set the upper limit at 10%.

The question whether there is direct desorption from α_1–$O_2(a)$ has been addressed by recording TOF-spectra at 153 K surface idle temperature. At this elevated temperature the mean residence time of an α_3–$O_2(a)$ or α_2–$O_2(a)$ molecule is estimated to be less than 1 or 200 ms, respectively. Using a low laser repetition rate oxygen molecules converted from α_1–$O_2(a)$ to α_2– and α_3–$O_2(a)$ will therefore desorb thermally between the laser shots. Any fast signal seen in the TOF-spectra must then originate directly from α_1–$O_2(a)$. The experiment yields a very small TOF signal. In time-of-flight it is present right from the first laser shots [Fig. 7(c)]. While the TOF-spectrum shows intensity at times corresponding to the fast channel [Fig. 6(c)], the spectrum is very broad and includes obviously a dominating contribution from thermal desorption. The tail of the TOF-spectrum falls off too slowly to be fit by a Maxwell–Boltzmann distribution. It can better be reconciled as thermal desorption spread out over a longer time period. The signal at short flight times indicates nonthermal desorption of O_2 from the α_1-state, but the cross section for this process must be much smaller than for the α_2-, α_3-state.

The angular distribution of molecules desorbing in the fast channel has been determined for desorption from the surface saturated at 90 K. For different angles θ of the QMS position with respect to the surface normal, the initial desorption yield is best fit by a $\cos^2 \theta$ function.

C. Dependence on the polarization of the radiation

In our study of NO_2 dissociation on a NO covered Pd(111) surface[7] we have proposed a method based on the

polarized nature of light to discriminate between substrate and localized adsorbate excitations as the initial step for a photochemical process on strongly absorbing, i.e., metal, surfaces. Chemisorbed molecular O_2 is an even better candidate for this method, because its binding geometry is known. Its surface photochemistry is frequently discussed as analogous to gas phase hydrogen peroxide, H_2O_2, photolysis. Gas phase photofragmentation of H_2O_2 has been studied in detail using sophisticated laser methods.[17,18] It is found that the electronic transition responsible for dissociation has predominantly perpendicular character, i.e., the electric field vector has to be perpendicular to the O–O axis to yield maximum transition probability.[19]

From the published values of the index of refraction of Pd[20] the absorption by the substrate can be calculated based on Fesnel's formulae.[21] Additionally the electric field components normal and parallel to the surface can be calculated.[22] The experimentally observed dependence of the yield on polarization and angle of incidence can then be compared to both the predictions based on absorption by the solid as well as with the expectations based on the surface electric fields which would interact with the transition dipole in the case of a localized excitation in the adsorbate–substrate complex.

Measurements of the desorption signal were performed as a function of angle of incidence and by switching between *s*- and *p*-polarization. The setup was the same as for the measurements of desorption yield as function of irradiation with the surface saturated at 90 K [Fig. 7(a)]. The mass spectrometer used for detection was simultaneously rotated with the crystal in order to keep the angle of detection with respect to the surface normal fixed. The recorded desorption signals were extrapolated to zero irradiation in order to avoid spurious effects due to the varying rate of coverage depletion. The resulting experimental data are plotted in Fig. 10 together with the absorptivity of palladium. For most angles three measurements on different days have been performed. The standard deviations are given with the data. In the lower panel we also show the signal ratios which have a better signal-to-noise because some systematic scatter is eliminated. Close agreement of the experimental results with the predictions of the model of bulk absorption is obtained, in particular with respect to the occurrence and height of the maximum at 50° in the data for *p*-polarization and to the signal ratios for both polarization cases.

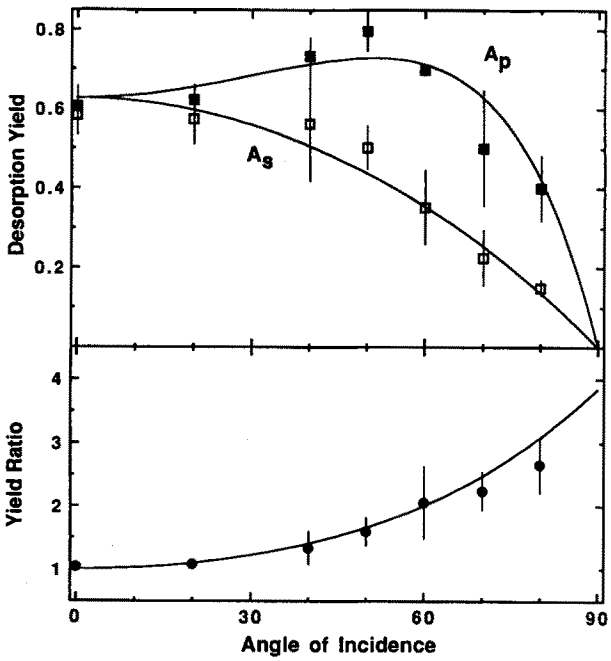

FIG. 10. Desorption yield for *s* (□) and *p* (■) polarization as a function of the angle of incidence. The error bars are obtained from the standard deviation of 2 or 3 measurements for each point. Within the error the data can only be described by a model which is based on the absorption in the metal substrate as the primary excitation step. The lower panel shows the ratios of the curves in the upper panel.

We have also compared TDS results obtained for normal and 60° off-normal irradiation. The angle and polarization dependence of these data is entirely consistent with the more carefully studied desorption yield. This indicates that the $\alpha_1 \rightarrow \alpha_2,\alpha_3$ conversion process is driven by the same kind of initial excitation as the desorption described in the previous paragraph.

Calculation of the field strength, on the other hand, shows that for both polarizations the component in the surface plane decreases monotonically with increasing angle of incidence, and in particular does not show a maximum at intermediate angles for *p*-polarization (Table II). A compo-

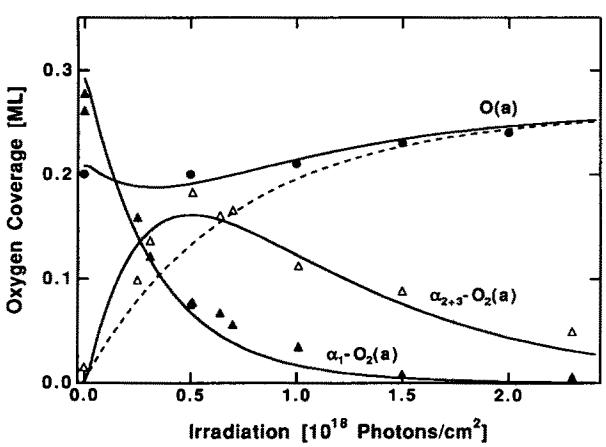

FIG. 9. Comparison of the TDS results for the α_1 prepared surface with a rate equation model: α_1–$O_2(a)$ (▲), α_{2+3}–$O_2(a)$ (△), total amount of atomic oxygen after annealing to 220 K (●). The solid curves give the results of the rate model. The dashed curve shows the calculated amount of photoinduced atomic oxygen.

TABLE II. Substrate absorptivity and surface electric field intensities $\langle E_i^2 \rangle$[a] at normal and 50° incidence (6.4 eV).

	Absorptivity		Field in surface plane		Field normal to surface	
	0°	50°	0°	50°	0°	50°
s	0.63	0.44	0.86	0.44	···	···
p	0.63	0.73	0.86	0.59	···	0.66

[a] The surface electric field strengths are calculated assuming unit intensity of the incident wave.

nent in the direction of the surface normal only exists for *p*-polarization and off-normal incidence. It is maximal at 50° incidence. The observed data cannot be reconciled with a transition dipole purely parallel or normal to the surface. From the observed signal at normal incidence it is evident that there would be a need for a contribution from the component in the surface. Based on our knowledge about gas phase H_2O_2 photolysis it must be assumed that a transition dipole perpendicular to the O–O bond will also contribute. In this case both the field strength normal to the surface and that in the plane, could contribute. The latter will be averaged over the various possible orientations of the dioxygen axis. If both field components contribute equally a 1:4.3 ratio would be predicted for 50° irradiation opposed to the 1:1.6 observed. We further note that any significant contribution from the electric field strength normal to the surface will lead to a ratio which is larger than the experimentally observed one, because already the in-plane components give a ratio of 1:1.35. But a strong contribution ($>50\%$ relative weight) from the normal component would be necessary to reproduce the observed maximum for *p*-polarization. But such a fit yields also rather unsatisfactory results with respect to the shape of the curve.

In conclusion, it turns out that the observed data cannot be fit with any simple model of a direct excitation of the adsorbate-substrate complex. It is on the other hand, very unlikely that the good fit by the bulk absorption curve is just accidental. There is, in fact, strong indication that substrate excitations drive at least the desorption from the saturated surface. We also note that the transition from π_1^* to σ^* which is proposed by Hanley *et al.* to be responsible for desorption from peroxo oxygen, for symmetry reasons can only be excited by that component of the electric field strength which is normal to the surface.

IV. DISCUSSION

A. Summary of photochemical processes observed

The presented TDS data are in complete agreement with the results reported by Hanley *et al.*[9] Three processes are evident: (1) photodesorption of $O_2(a)$, (2) conversion from α_1–$O_2(a)$ to α_2,α_3–$O_2(a)$ and (3) photodissociation of $O_2(a)$ to form atomic oxygen. The observation of a desorption channel with nonthermal translational energies clearly indicates the photochemical character of the first process. The observed preferred depletion of higher binding energy states, by dissociation or desorption, is on first sight in contrast to intuitive thermodynamic arguments that the system should relax with the strongest bound states occupied, which are also filled first in adsorption. It therefore needs further explanation by other processes.

The third process, formation of atomic oxygen is difficult to quantify experimentally because in TDS atomic oxygen is also formed thermally when the temperature is elevated above 180 K. Hence the finally detected atomic oxygen will always be the sum from both processes. Because the saturation coverage of atomic oxygen is smaller than the saturation coverage of molecular oxygen, the formation of $O(a)$ will be limited by the saturation of available sites. It is therefore extremely likely that those sites which are not filled by photochemically produced atomic oxygen will be filled through thermal dissociation during TDS resulting in the same total amount as long as that produced photochemically does not exceed the maximum which can be formed during TDS. Therefore the small increase of atomic oxygen seen in postirradiation TDS will most probably strongly underestimate the efficiency of photolysis. In those studies, which have directly monitored the formation of atomic oxygen by HREELS,[10,14] dissociation into atomic oxygen was seen as a direct photoinduced process. The just discussed thermal dissociation of $O_2(a)$ in TDS also implies that the apparent population of α_1–$O_2(a)$ seen in TDS will underestimate the real population.

From the presented data the following picture evolves. Irradiation of α_1–$O_2(a)$ yields a small signal of nonthermal O_2 desorption. Conversion to α_2,α_3–$O_2(a)$ is the dominant process. Irradiation of α_2,α_3–$O_2(a)$ (because of the close desorption temperature it was not possible to prepare these states separately) yields a strong nonthermal desorption signal. From the saturated surface a slow, thermal desorption process is also observed during that time in which α_1–$O_2(a)$ is converted to α_2,α_3–$O_2(a)$. Matsushima[11] noted that preadsorbed oxgygen drastically reduces the saturation coverage of molecular oxygen, especially in the α_1 state. We therefore suggest to identify the formation of atomic oxygen as the common driving force for the observed conversion between binding states as well as the release of molecules in the slow channel. The latter process happens only at high coverages because the newly formed atomic oxygen competes with the molecular species for binding sites. Molecular oxygen released by such a displacement process desorbs accommodated to the surface temperature.

B. Reaction model

In the following a simple reaction model for the photoinduced processes in the O_2/Pd(111) system will be presented. In order to simplify the picture and to reduce the number of necessary variables we will combine the α_2 and α_3 oxygen species and neglect the conversion process between them. The maximum coverage in the α_1 state, $[O_{2,\alpha_1}]_{max}$, depends on the coverage of atomic oxygen, [O], according to the empirically obtained relationship[11]

$$[O_{2,\alpha_1}]_{max} = [O_{2,\alpha_1}]_0 \cdot \left(1 - {}^{[O]}/_{[O]_{max}}\right)^2, \qquad (2)$$

where $[O_{2,\alpha_1}]_0$ is the α_1 saturation coverage on the clean surface and $[O]_{max}$ the saturation coverage of atomic oxygen. Photolytically formed atomic oxygen leads to a drastic reduction of the maximum α_1 coverage. In our model we will therefore interpret the conversion feature observed in TDS as a displacement process induced by photodissociation of $O_2(a)$. It is assumed that the photoinduced desorption and dissociation reactions proceed via the following steps

$$O_{2,\alpha_1}(a) \xrightarrow{h\nu} O_2(\uparrow)_{\text{fast}} \quad (3)$$
$$\xrightarrow{h\nu} 2O(a),$$

$$O_{2,\alpha_{2,3}}(a) \xrightarrow{h\nu} O_2(\uparrow)_{\text{fast}} \quad (4)$$
$$\xrightarrow{h\nu} 2O(a)$$

and

$$O(a) + O_{2,\alpha_1}(a) \rightarrow O(a) + O_{2,\text{displaced}}, \quad (5)$$

where $O_2(\uparrow)_{\text{fast}}$ is the nonthermally desorbed O_2. $O_{2,\text{displaced}}$ denotes the α_1 oxygen which exceeds the maximum coverage given by Eq. (2). The displaced oxygen will either be converted into the α_2 and α_3 states if there are enough empty binding sites, or has to desorb otherwise, i.e.,

$$O_{2,\text{displaced}} \rightarrow O_{2,\alpha_{2,3}}(a)$$
$$\rightarrow O_2(\uparrow)_{\text{slow}}. \quad (6)$$

The desorbing fraction of $O_{2,\text{displaced}}$ will be accommodated to the surface temperature in the translational degree of freedom. This fraction of O_2 leaving the surface manifests itself as the slow component of the TOF spectra, $O_2(\uparrow)_{\text{slow}}$, whereas the direct photodesorption yields the fast component, $O_2(\uparrow)_{\text{fast}}$.

We introduce the function

$$f([O]) = \left(1 - {}^{[O]}/_{[O]_{\max}}\right) \quad (7)$$

to simplify the further writing. Assuming first order reactions, we obtain the following rate equations,

$$\frac{d}{dt}[O_{2,\alpha_1}] = -(k_{\text{des1}} + k_{\text{diss1}} f([O]))[O_{2,\alpha_1}]$$
$$- k_d [O_{2,\alpha_1}]_{\text{displaced}} \quad (8)$$

$$\frac{d}{dt}[O_{2,\alpha_{2,3}}] = -(k_{\text{des2,3}} + k_{\text{diss2,3}} f([O]))[O_{2,\alpha_{2,3}}]$$
$$+ k_d [O_{2,\alpha_1}]_{\text{converted}} \quad (9)$$

$$\frac{d}{dt}[O] = 2(k_{\text{diss1}}[O_{2,\alpha_1}] + k_{\text{diss2,3}}[O_{2,\alpha_1}]) f([O]), \quad (10)$$

where k_{des} and k_{diss} are the rate constants for photodesorption and photodissociation, respectively. The factor $f([O])$ in the those terms which describe the dissociation reflects the necessary availability of one additional empty site for the dissociation. k_d denotes the rate for the displacement process, which is considered to be much faster than the other processes so that its turnover is quasi-instantaneously. The resulting rate equation for the desorption of O_2 has two contributions, one from direct photodissociation and one from displaced oxygen:

$$\frac{d}{dt}[O_2(\uparrow)_{\text{fast}}] = k_{\text{des1}}[O_{2,\alpha_1}] + k_{\text{des2,3}}[O_{2,\alpha_{2,3}}] \quad (11)$$

$$\frac{d}{dt}[O_2(\uparrow)_{\text{slow}}] = k_d([O_{2,\alpha_1}]_{\text{displaced}}$$
$$- [O_{2,\alpha_1}]_{\text{converted}}). \quad (12)$$

We used the following abbreviations

$$[O_{2,\alpha_1}]_{\text{displaced}} = g([O_{2,\alpha_1}] - [O_{2,\alpha_1}]_0 f([O])^2)$$
$$g(x) = \begin{cases} x & \text{if } x > 0 \\ 0 & \text{if } x \leqslant 0 \end{cases} \quad (13)$$

$$[O_{2,\alpha_1}]_{\text{converted}} = [O_{2,\alpha_1}]_{\text{displaced}}$$
$$- g([O_2] - [O_2]_0 f([O])), \quad (14)$$

where $[O_2]$ is the total oxygen coverage with $[O_2]_0 = 0.62$ ML. We note that $[O_{2,\alpha_1}]_{\text{converted}}$ is always positive or zero. In Eq. (14) a linear dependence on $f([O])$ has been chosen because the maximum coverage decreases slower for O_2 than for O_{2,α_1}.

For a given initial O_2 coverage and a chosen set of rate constants the time evolution of these equations can be readily obtained by numerical propagation. We can explain the main features of the observed desorption yields as well as the TDS results using only three rate constants, k_{des1}, $k_{\text{des2,3}}$ and $k_{\text{diss}} = k_{\text{diss1}} = k_{\text{diss2,3}}$. Because no experimental data are available detailing the different cross sections for dissociation from α_1 and $\alpha_{2,3}$ binding sites, we assumed the two constants are equal. The obtained rate constants can be converted to cross sections by

$$\sigma = \frac{k}{F_{\text{ph}}}, \quad (15)$$

where F_{ph} is the photon flux. From the best fit to all data with one set of rate constants we obtain for the desorption cross sections $\sigma_{\text{des1}} = 0.2 \cdot 10^{-18}$ cm^2 and $\sigma_{\text{des2,3}} = 1.05 \cdot 10^{-18}$ cm^2 and for the dissociation cross section $\sigma_{\text{diss}} = 0.55 \cdot 10^{-18}$ cm^2.

The results of such a numerical simulation according to Eqs. (8)–(12) are shown as the solid curves in Figs. 7 and 8–9 for the yields and the TDS results, respectively. The desorption yields in the fast TOF component are well reproduced by the model (Fig. 7). For an initially saturated surface we obtain also a slow component, again in agreement with the experimental findings. If initially only α_1 is populated, all displaced oxygen is converted, because there are always sufficient empty sites available. Therefore no slow channel is present. The yield in the fast channel increases as the adsorbate is converted from α_1– to $\alpha_{2,3}$–$O_2(a)$. For 153 K surface temperature we assumed that all $\alpha_{2,3}$–$O_2(a)$ will-desorb thermally between two laser shots [Fig. 7(c)]. Figures 8 and 9 show a comparison of the modelled α_1 and $\alpha_{2,3}$ coverages and the corresponding TDS features. The plotted α_1 coverage is corrected for thermal dissociation during TDS. Up to an exposure of $0.5 \cdot 10^{18}$ photons/cm^2 the conversion process for the saturated surface (Fig. 8) seems to be slightly overestimated, which coincides with the too rapid decrease of the slow channel in Fig. 7(a). The TDS data for

TABLE III. Cross sections obtained from the reaction model.

		Cross section [10^{-18} cm^2]
Dissociation	k_{diss}	0.55
Desorption from α_1	k_{des1}	0.2
Desorption from α_{2+3}	$k_{\text{des2,3}}$	1.05

atomic oxygen, as titrated by CO oxidation, are also shown. The dashed line corresponds to the calculated amount of photodissociated oxygen, whereas the solid line includes also the thermal dissociation of α_1–O_2 above 180 K. After irradiation with 10^{18} photons/cm^2 the atomic oxygen on the surface is mainly of photochemical origin. We set the maximum coverage of atomic oxygen to $[O]_{max} = 0.3$ ML, which would be in agreement with the maximum value of 0.32 ML obtained by electron bombardment.[23]

It should be pointed out that we have described the photochemistry of the α_2 and α_3 oxygen species only by effective cross sections. Nevertheless, we believe the proposed reaction scheme to be the simplest picture which can explain our results at least semiquantitatively. The obtained cross sections for desorption increase with decreasing binding energy of the oxygen species, in agreement with general experience.

C. Mechanism of photochemical processes

The cross sections determined in the present work can readily be reconciled with the numbers given by Hanley *et al.*[9] They report from the threshold at $h\nu = 3.5 \pm .4$ eV to the highest photon energy applied, 5.2 eV, a constant increase to $1.3 \cdot 10^{-19}$ and $3.5 \cdot 10^{-19}$ cm^2 for photodesorption and dissociation, respectively. Our numbers are by a factor of 10 larger than these values and may be considered as continuation of the increasing cross sections from their threshold towards higher photon energies.

Two mechanisms have recently been discussed with regard to photochemistry on metal surfaces: Photolysis might originate from excitation of valence electrons of adsorbed dioxygen or be stimulated by excitation of the palladium substrate. The absorptivity of palladium in the UV is considerable and therefore, substantial excitation of substrate electrons occurs within the penetration depth of the light (~ 100 Å). The work function of Pd(111) is 5.5 eV[24] and increases by 0.95 and 0.6 eV for the molecular oxygen covered and atomic oxygen covered surface, respectively.[9] Our photon energy is between these energies, i.e., a broad distribution of excited substrate electrons will be generated reaching up to and above the vacuum level. Excited electrons can diffuse to the surface and they may occupy unfilled orbitals of the adsorbate complex, eventually leading to bond cleavage if these orbitals are antibonding with respect to the O–O bond or the O_2–Pd bond.

Hanley *et al.* discuss the photochemistry of dioxygen in the framework of the "frontier orbital" approach[25] and postulate that all processes should be initiated by direct excitations of the substrate–adsorbate complex except the dissociation of peroxo which should be stimulated by substrate excitations. However, our data on the polarization dependence of the desorption yield from the saturated surface, probing desorption from the $\alpha_{2,3}$–$O_2(a)$ states, indicate that substrate excitations are, under these conditions, the dominant primary excitation step. Supplementary TDS data indicate that the other processes follow the same dependence, but further experimental work is required to elucidate especially the mechanistics of the $O_2(a)$ dissociation.

We also note that the observed wavelength dependence follows the increase of the absorptivity of Pd in the UV.[20] The observed increase in cross section is steeper than that for light absorption. This is, however, not too surprising if one takes into account that higher energy electron excitations might have a higher probability of causing chemistry. Pd exhibits an electronic resonance at 7.5 eV[26,27,28] which is in some part of the literature identified with a surface plasmon.[29] Imbihl *et al.*[12] have reported a resonant excitation of the O–O stretching mode in EELS peaking at energies below 3 eV, which was the minimum energy experimentally feasible in that work. In summary there is substantial evidence that substrate excitations can play a strong role in the UV-photochemistry of O_2 on Pd. This is in agreement with the findings of Hatch *et al.*[14] for the system O_2/Ag(110) where the lack of any azimutal dependence when rotating the polarization at normal incidence clearly indicated that also there substrate excitations are dominant.

The experimentally observed translation energy, $\langle E_{trans} \rangle / 2k$, of 800 K for the "fast" channel is far in excess of the surface temperature excluding any explanations based on local substrate heating. This nonthermal energy indicates that after some possible intermediate excitation steps the O_2 molecule must become excited onto the repulsive branch of a potential energy surface from which it then desorbs. But it is only a minor fraction of the electronic excitation (6.4 eV) which is converted into translational energy. This can be rationalized in the framework of the Menzel–Gomer–Redhead (MGR) model,[30,31] as indicating a strong competition between desorption and quenching as a consequence of a short lifetime on the excited surface so that only a small amount of potential energy is converted to translational energy. This is also consistent with the observed larger desorption cross section from the weaker bound $\alpha_{2,3}O_2(a)$ species for which, within the MGR model, a shorter lifetime suffices to collect enough translational energy to overcome the ground state potential well. The observed order of magnitude of the translational energy is in agreement with general experience with laser induced desorption from metallic surfaces.[5,6] It is worthwhile noting that the cross sections observed in this work for O_2 are 3–4 orders of magnitude larger than those reported for photoinduced desorption of NO from Pt[6] and Pd[7] in the same photon energy regime.

V. CONCLUSION

The results reported here can be summarized as follows:

(1) Upon UV irradiation with 6.4 eV photons molecular oxygen absorbed on Pd(111) undergoes dissociation, desorption and conversion between binding states.

(2) Time-of-flight spectroscopy shows that desorption is nonthermal leading to the ejection of O_2 molecules with a translational energy, $\langle E_{trans} \rangle / 2k$, of 800 ± 50 K.

(3) From the saturated surface additional O_2 desorption in a "slow" channel is seen with a translational energy corresponding to the surface temperature. This channel is only populated under conditions for which both formation of atomic oxygen and conversion between binding sites occurs.

(4) The experimental observations can be reproduced by a simple model which takes into account nonthermal de-

sorption, dissociation to form atomic oxygen and displacement processes which are caused by the reduction of the maximum molecular oxygen coverage due to the accumulation of atomic oxygen. Analysis of the experimental data on the basis of this model yields cross sections for dissociation of $0.55 \cdot 10^{-18}$ cm^2 and for desorption from α_1 and $\alpha_{2,3}$ oxygen of $0.2 \cdot 10^{-18}$ and $1.05 \cdot 10^{-18}$ cm^2, respectively.

(5) The dependence of the desorption yield on angle of incidence and polarization indicates that substrate excitations are the dominant primary excitation step, at least for desorption from $\alpha_{2,3}$-oxygen.

Note added in proof: After submission of this paper we learned that Yoshinobu *et al.* [Chem. Phys. Lett. **169**, 209 (1990)] also studied the polarization dependence of the O_2 desorption yield on Pd(111) and found for the angle tested, 60°, values whose ratio is in good agreement with our data.

ACKNOWLEDGMENTS

We thank Albert Cassuto and Stefan Nettesheim for many fruitful discussions and experimental help during the initial stages of this work. J.M.W. acknowledges a senior scientist fellowship by the Alexander von Humboldt Stiftung.

[1]P. Avouris and R. E. Walkup, Ann. Rev. Phys. Chem. **40**, 173 (1989).
[2]W. Ho, in *Desorption Induced by Electronic Transitions, DIET IV*, Springer Series in Surface Science (Springer, Berlin, 1990).
[3]S. A. Costello, B. Roop, Z. M. Liu, and J. M. White, J. Phys. Chem. **92**, 1019 (1988). Z.-M. Liu, S. A. Costello, B. Roop, S. R. Coon, S. Akhter, and J. M. White, J. Phys. Chem. **93**, 7681 (1989); B. Roop, K. G. Lloyd, S. A. Costello, A. Campion, and J. M. White, J. Chem. Phys. **91**, 5103 (1989).
[4]E. P. Marsh, M. R. Schneider, T. L. Gilton, F. L. Tabares, W. Meier, and J. P. Cowin, Phys. Rev. Lett. **60**, 2551 (1988).
[5]F Budde, A. V. Hamza, P. M. Ferm, D. Weide, P. Andresen, and H. J. Freund, Phys. Rev. Lett. **60**, 1518 (1988); P. M. Ferm, F. Budde, A. V. Hamza, S. Jakubith, G. Ertl, D. Weide, P. Andresen, and H.-J. Freund, Surf. Sci. **218**, 467 (1989).
[6]S. A. Buntin, L. J. Richter, R. R. Cavanagh, and D. S. King, Phys. Rev. Lett. **61**, 1321 (1988); S. A. Buntin, L. J. Richter, D. S. King, and R. R. Cavanagh, J. Chem. Phys. **91**, 6429 (1989).
[7]E. Hasselbrink, S. Jakubith, S. Nettesheim, M. Wolf, A. Cassuto, and G. Ertl, J. Chem. Phys. **92**, 3154 (1990).
[8]S. K. So, R. Franchy, and W. Ho, J. Chem. Phys. **91**, 5701 (1989).
[9]L. Hanley, X. Guo, and J. T. Yates, Jr., J. Chem. Phys. **91**, 7220 (1989).
[10]X.-Y. Zhu, S. R. Hatch, A. Campion, and J. M. White, J. Chem. Phys. **91**, 5011 (1989).
[11]T. Matsushima, Surf. Sci. **157**, 297 (1985).
[12]R. Imbihl and J. E. Demuth, Surf. Sci. **173**, 395 (1986).
[13]X. Guo, A. Hoffman, and J. T. Yates, Jr., J. Chem. Phys. **90**, 5787 (1989).
[14]S. R. Hatch, X.-Y. Zhu, J. M. White, and A. Campion, J. Chem. Phys. **92**, 2681 (1990).
[15]D. Burgess, Jr., P. C. Stair, and E. Weitz, J. Vac. Sci. Technol. A **4**, 1362 (1986).
[16]W. L. Guthrie, T.-H. Lin, S. T. Ceyer, and G. A. Samorjai, J. Chem. Phys. **76**, 6398 (1982).
[17]G. Ondrey, N. van Veen, and R. Bersohn, J. Chem. Phys. **78**, 3732 (1983).
[18]K.-H. Gericke, S. Klee, F. J. Comes, and R. N. Dixon, J. Chem. Phys. **85**, 4463 (1986).
[19]S. Klee, K.-H. Gericke, and F. J. Comes, J. Chem. Phys. **85**, 40 (1986).
[20]*Physik Daten, Vol. 18-1*, edited by H. Behrens and G. Ebel, (Fachinformationszentrum, Karlsruhe, 1981).
[21]M. Born and E. Wolf, *Principles of Optics*, (Pergamon Press, Oxford, 1980).
[22]W. N. Hansen, J. Opt. Soc. Am. **58**, 380 (1968).
[23]A. Hoffman, X. Guo, and J. T. Yates, Jr., J. Chem. Phys. **90**, 5793 (1989).
[24]G. D. Kubiak, J. Vac. Sci. Technol. A **5**, 731 (1987).
[25]R. Hoffmann, Rev. Mod. Phys. **60**, 601 (1988).
[26]N. E. Christensen, Phys. Rev. B **14**, 3446 (1976).
[27]S. Robin, in *Optical properties and electronic structure of metals and alloys*, edited by Ed Abeles, (North Holland, Amsterdam, 1966).
[28]P. Legare, Y. Holl, and G. Maire, Solid State Commun. **31**, 307 (1979).
[29]S. D. Bader, J. M. Blakely, M. B. Brodsky, R. J. Friddle, and R. L. Panosh, Surf. Sci. **74**, 405 (1978).
[30]D. Menzel and R. Gomer, J. Chem. Phys. **41**, 3311 (1964).
[31]P. A. Redhead, Can. J. Phys. **42**, 886 (1964).